

Realization and optimization of thermoelectric devices using bismuth and antimony materials

G. Savelli^{1,2}, M. Plissonnier¹, J. Bablet¹, C. Salvi¹, J.M. Fournier^{1,2}
¹CEA/LITEN/DTNM/LCH, 17 rue des Martyrs, 38054 Grenoble Cedex 9, France
²LEG, CNRS UMR 552, BP 46, 38402 St Martin d'Hères Cedex, France

Abstract

In recent years, microelectronics has contributed to the development of complex and varied technologies. Many of these technologies can be applied successfully to realize Seebeck micro generators: photolithography and deposition methods allow the elaboration of thin thermoelectric structures at the micro-scale level.

Our goal is to scavenge energy by developing a miniature power source for operating electronic components. First Bi and Sb micro-devices on glass substrate have been manufactured with an area of 1cm^2 including more than one hundred junctions. We have optimized each step of the manufacturing process: photolithography, deposition process, annealing conditions and metallic connections. Three different device structures have been realized with differing micro-line dimensions. Each device performance will be reviewed and discussed as a function of their design structure.

Introduction

Since the last decade, there is a growing interest in wireless sensor nodes with the goal of monitoring human environments. Because advances in low power VLSI design and CMOS fabrication have dramatically decreased the power requirements of sensors, it is now possible to consider self-powered systems in sensor nodes [1].

At the same time, the interest in producing micro-electromechanical systems (MEMS) opens new opportunities in the field of micro power generation. Micro thermoelectric converters are a promising technology due to their high reliability and quiet operation, and the fact that they are usually environmentally friendly. The efficiency of a thermoelectric device is generally limited to its associated Carnot Cycle efficiency reduced by a factor which is dependent upon the thermoelectric figure of merit (ZT) of the materials [2] used in the thermoelectric device. Recent developments in micro-thermoelectric devices using thin film deposition technology [3] have shown that energy scavenged from human environment (low thermal gradient) covers the sensor's power need.

The thermoelectric materials (TE) used in this study are bismuth and antimony. Both Bi and Sb are semimetals, that is, there is an energy overlap between the valence and conduction bands. Near room temperature, the thermoelectric power (or Seebeck coefficient) of both Bi and Sb are small enough: typical values are about $-70\mu\text{V.K}^{-1}$ for Bi and $40\mu\text{V.K}^{-1}$ for Sb [4]. Nevertheless, the experience we have acquired with these common thermoelectric materials will be useful for our current device improvements with more competitive thermoelectric materials.

In this paper we review a wafer technology approach to manufacture a thermoelectric device. Design and technological process steps will be identified in order to

propose a strategy to manufacture thermoelectric converters (TEC).

Experimental

1. Device description

We use a four inches glass substrate. 42 devices and 6 test areas are distributed on it. Figure 1 shows this Bi-Sb prototype.

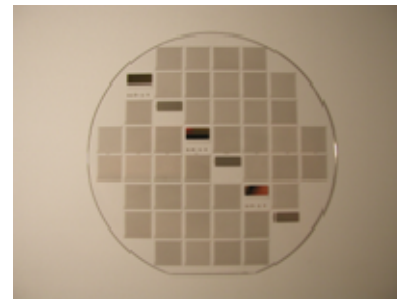


Figure 1: Bi-Sb device realized by microelectronic technologies: PVD deposition, photolithography....

Dimension of chips is $1\times 1\text{cm}^2$, bismuth and antimony line widths are 20, 30 or $40\mu\text{m}$, spaced by $20\mu\text{m}$.

This geometry is obtained by photolithography with a series of 3 masks.

These geometry allow us to obtain 250 lines (125 of bismuth and 125 of antimony in alternation), i.e. 125 junctions for the 20×20 chips, 208 lines and 104 junctions for the 30×20 chips and 166 lines and 83 junctions for the 40×20 chips.

Moreover Bi and Sb lines are electrically connected in series by using Ti and Au metallic junctions. Fig.2. shows these lines in detail and an enlargement of the metallic connections.

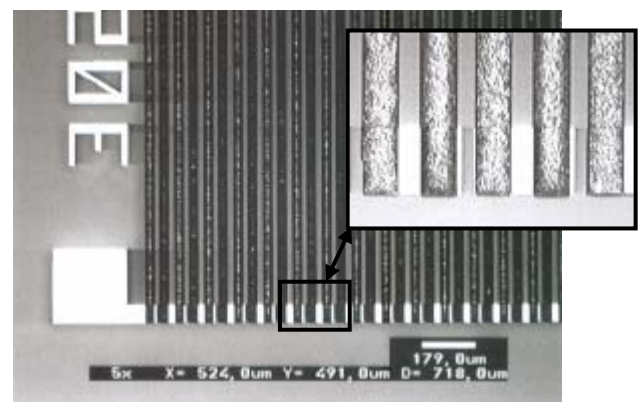


Figure 2: Bismuth and antimony lines with electrical connections.

Bismuth and antimony lines, and titanium and gold connections are deposited by sputtering PVD (Physical Vapor Deposition). The reason for the choice of the deposition method is explained below. The sputtering process use six inches targets for best thickness uniformity. Each deposition is carried out in Ar atmosphere at 1.2 Pa. In addition, an rf generator provides power supplies from 0 to 300W and operates at a frequency of 13.56MHz.

Also it is necessary to add adhesion layers for bismuth and antimony deposition. These sublayers permit Bi and Sb to adhere to the substrate during photolithography operations (resin addition, etching...). A flash Ti adhesion layer (1nm) is used for Bi lines and flash Ti+Au adhesion layers (1nm+1nm) are used for Sb lines. We will show in part 3. of this paper that these added layers have no influence on both thermoelectric properties and crystallographic structures.

2. Device treatment and characterization

Annealing is the crucial point for this device. Indeed in thermoelectrics, it is important to obtain the lowest electrical resistivity. To achieve these lowest values a high layer quality is necessary. But, for example, bismuth is well known to deposit in the form of grains [5-6] which increases resistivity. The objective is thus to improve layer homogeneity, and so to reduce grains size. Sputtering deposition is used because it allows to obtain smaller grain sizes than evaporation deposition, and so to obtain thin films which are more continuous and uniform [5]. Furthermore different annealing conditions have been studied to reduce grain size. Two kinds of annealing will be compared in section 3: annealing by furnace and by laser. Annealing by furnace is carried out at 260°C for bismuth ($T_m[\text{Bi-Ti}] = T_m[\text{Bi}] = 271^\circ\text{C}$) and 355°C for antimony ($T_m[\text{Sb-Au}] = 360^\circ\text{C}$) in Ar atmosphere for 8 hours (T_m are obtained from Binary Alloy Phase Diagrams). Annealing by laser achieved using a Xe-Cl excimer laser with 200ns of pulse width and a wavelength of 308nm.

To analyze the performance of our devices, we use several characterization tools: Scanning Electron Microscopy (SEM) to check geometry dimensions and photolithography quality, X-ray diffraction to analyze crystallographic structure of bismuth and antimony, a four probe method is used to measure electrical resistivity, and a thermoelectric characterization tool which provides us with Seebeck coefficient and useful electrical power.

Results

1. Influence of annealing

In this part, we present results obtained before and after annealing and compare the two methods. Here crystallographic structures and electrical resistivity are studied. First, the influence of annealing on bismuth lines is tested.

As Bi layers are “granular”, resistivity is too high. Thus Bi resistivity before annealing is $1600\mu\Omega\cdot\text{cm}$.

To reduce this value, we tested two kinds of annealing. Figure 3 shows Bi lines before and after the two kinds of annealing (on Fig.3. only Bi lines are deposited).

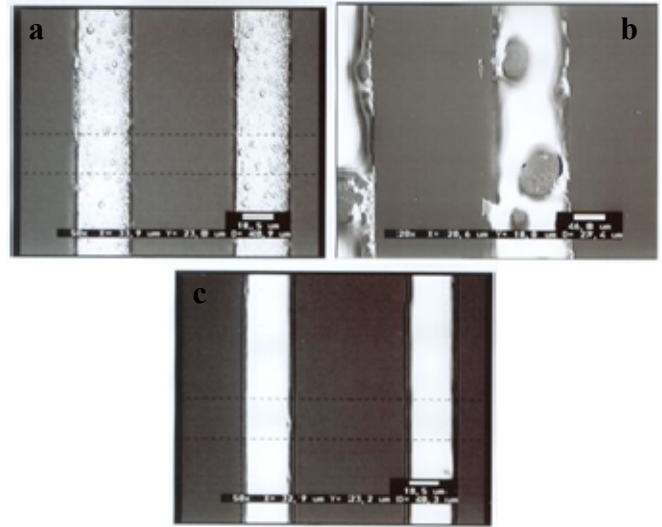


Figure 3: Influence of annealing on Bi lines - a: without annealing - b: annealing by furnace at 260°C - c: annealing by laser.

Figure 3a confirms the granular aspect of Bi lines. We can see in Figure 3b that some parts of lines have melted originating important discontinuities in lines. Resistivity after annealing by furnace (at 260°C for 8 hours) decreases to $900\mu\Omega\cdot\text{cm}$.

Figure 3c shows Bi lines after annealing by laser. The granular aspect seems to have disappeared. Figure 4 shows the influence of the annealing by laser.

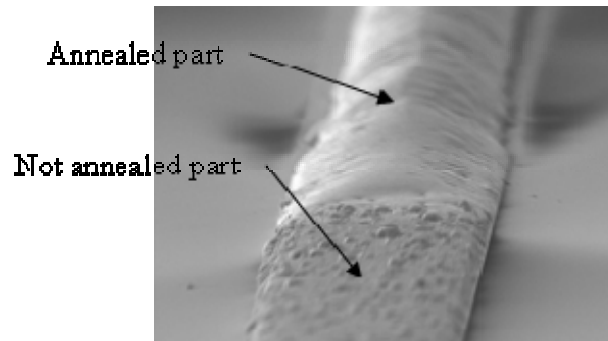


Figure 4: Bi line: one part is annealed by laser, not the other one (photo realized by SEM).

On Figure 4 we annealed only part of the line. We see that grains disappeared on the annealed part. Figure 5 shows a cross-section of the line (annealed part): absence of grains is confirmed.

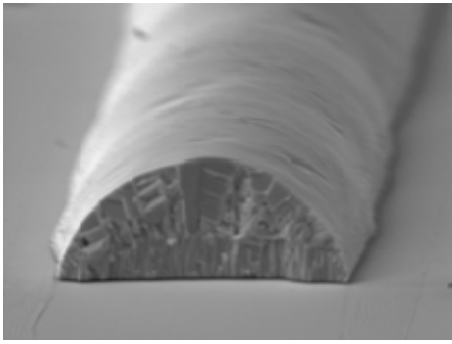


Figure 5: Cross section of the Bi annealed line (SEM photograph).

The granular aspect of Bi layer is reduced. This is also confirmed by resistivity measurements. We obtain a resistivity of $800\mu\Omega\cdot\text{cm}$ after annealing by laser.

Annealing influence on Sb layers is also reviewed with different annealing conditions. Deposited Sb resistivity is $1100\mu\Omega\cdot\text{cm}$. After annealing at 355°C for 8 hours, its resistivity decreases to $825\mu\Omega\cdot\text{cm}$. There is no notable improvement after an annealing by laser, its resistivity is $825\mu\Omega\cdot\text{cm}$, too.

Figure 6 shows two lines, one of bismuth and one of antimony, where each line has an annealed part and not the other one.

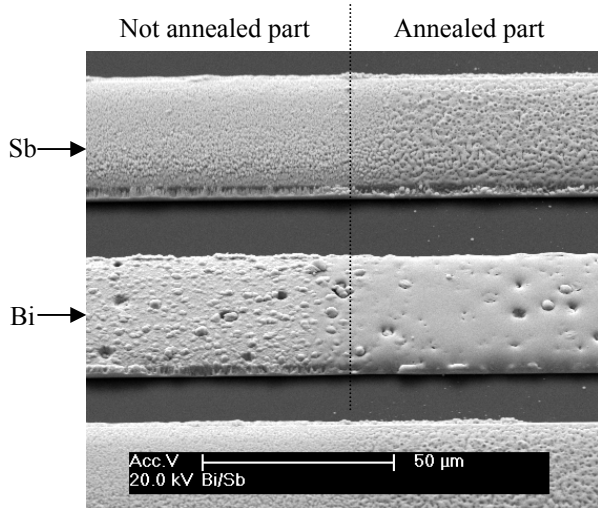


Figure 6: Influence of annealing by laser on both Bi and Sb lines.

We always see that Bi granular aspect disappears and that there is no important visible change in the Sb layer. To confirm these observations, Figure 7 presents bismuth and antimony X-ray diffraction spectra.

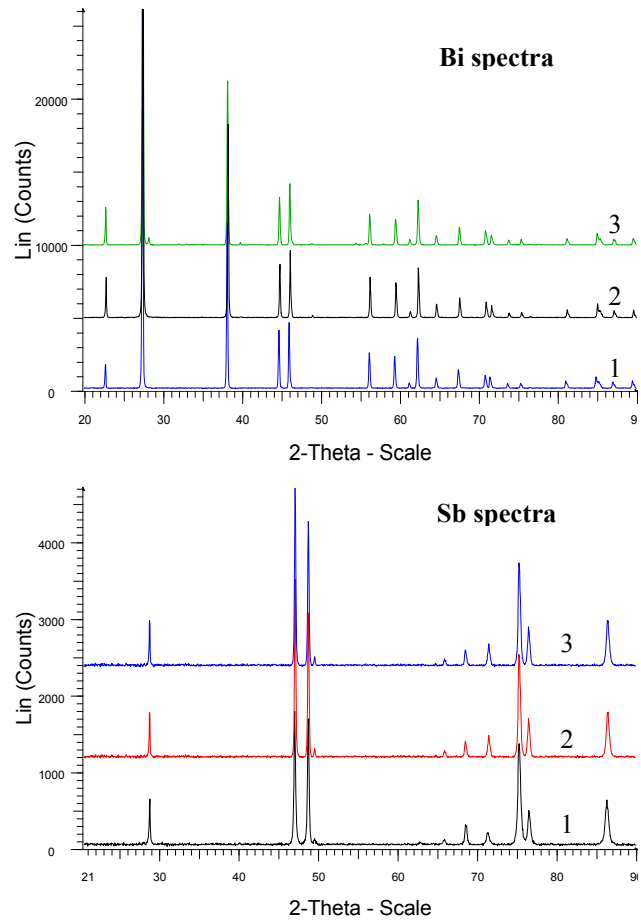


Figure 7: Bi and Sb X-rays spectra - 1: without annealing - 2: after annealing by laser - 3: after annealing by furnace.

We obtain a good crystallographic structure, i.e. a rhombohedral structure for bismuth films. All peaks are identified by the JCPDS files. These parameters are: $a=b=4.547\text{\AA}$, $c=11.8616\text{\AA}$, and $\alpha=\beta=90^\circ$, $\gamma=120^\circ$. For antimony films, we obtain a rhombohedral structure too. In the same way, its structure is identified by the JCPDS files, with the following parameters: $a=b=4.307\text{\AA}$, $c=11.273\text{\AA}$, and $\alpha=\beta=90^\circ$, $\gamma=120^\circ$.

These spectra show that Bi and Sb annealing by laser doesn't disturb the initial polycrystalline structure. This is an essential point, because this structure, which can be considered as a slightly distorted cube, is responsible for a minute band overlap, leading to the presence of small and equal electron and hole densities at all temperatures [7]. Moreover, no peaks associated with titanium or gold were detected, indicating that no Bi-Ti or Sb-Au alloy appeared during the annealing process.

Figure 8 summarizes resistivity results for Bi and Sb, with and without annealing.

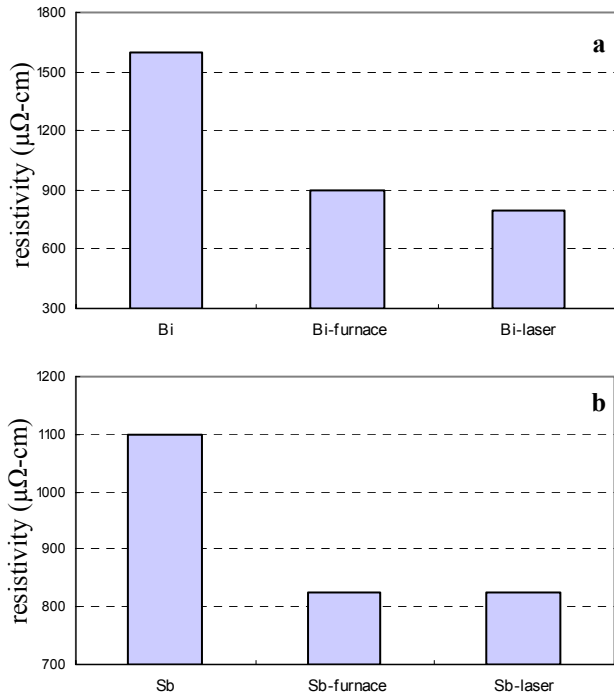


Figure 8: Influence of annealing on electrical resistivity - a: for Bi lines - b: for Sb lines.

Finally, we annealed the device at 240°C for 9 hours in Ar atmosphere to improve interface layers and to stabilize the device.

3.2. Thermoelectric properties

Thermoelectric generators are characterized by the Seebeck voltage V_s and the useful electrical power P_u , defined by the following equations:

$$P_{sc} = \frac{V_s^2}{R_g} \quad ; \quad P_u = \frac{P_{sc}}{4} \quad (\text{eq.1})$$

$$R_g = N \left[\rho_{Bi} \frac{L_{Bi}}{A_{Bi}} + \rho_{Sb} \frac{L_{Sb}}{A_{Sb}} + 2 \rho_m \frac{L_m}{A_m} \right] \quad (\text{eq.2})$$

$$R_g \approx N \left[\rho_{Bi} \frac{L_{Bi}}{A_{Bi}} + \rho_{Sb} \frac{L_{Sb}}{A_{Sb}} \right] \quad \text{with } \rho_m \ll \rho_{Bi} \text{ and } \rho_{Sb}$$

where P_{sc} is the short-circuit power, R_g is the chip global electrical resistance, N is the total junctions number for one chip, ρ is the electrical resistivity, L is the line length and A the line section area. Metallic-TE materials contact resistance is here negligible compared to the global lines resistance.

V_s depends on Seebeck coefficient (or thermoelectric power S) and the number of electrically connected junctions in series. Thus V_s increases when lines density increases. In the same way, useful electrical power P_u depends on V_s and R_g (eq.1). In that case, lines geometry affects P_u directly.

Table 1 shows R_g values for each device geometry: $R_{g \text{ theo.}}$ is calculated with bulk material resistivity ($\rho_{Bi}=117\mu\Omega\cdot\text{cm}$, $\rho_{Sb}=40.1\mu\Omega\cdot\text{cm}$ at 300K and ρ_m is the metallic junctions resistivity). $R_{g \text{ cal.}}$ is calculated with experimentally measured Bi-Sb resistivity (i.e. after annealing by laser). For the calculation, we used eq.2, and $R_{g \text{ eff.}}$ is the effective device electrical resistance after the last annealing. As expected, R_g depends strongly on lines geometry and lines density.

	20x20	30x20	40x20
N	125	104	83
$R_{g \text{ theo.}}$ (k Ω)	17,8	9,9	5,9
$R_{g \text{ cal.}}$ (k Ω)	184,7	102,4	61,3
$R_{g \text{ eff.}}$ (k Ω)	82	63,8	31

Table 1: Comparison of R_g values using different resistivity values.

The results show that annealing process is critical in order to decrease R_g to the minimal value $R_{g \text{ theo.}}$. The last annealing gave a decrease of 55% of the chip global resistance. Moreover, R_g values decrease normally with increasing line widths (and so decreasing number of lines).

Figure 9 shows the useful electric power P_u calculated using these different values of R_g for the 40x20 device as a function of temperature difference.

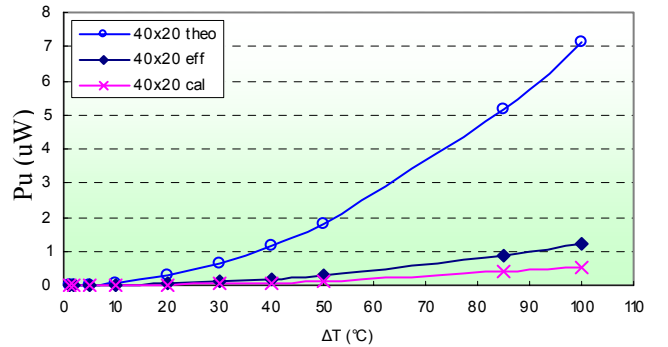


Figure 9: Useful electrical power P_u as a function of temperature difference.

This graph shows that using bulk material resistivity values, we can obtain 7.2 μW for $\Delta T=100\text{K}$. Without the last annealing we obtain 0.65 μW and with the last annealing, we obtain 1.2 μW for $\Delta T=100\text{K}$, that is an increase of nearly 50%.

It is interesting to compare the Seebeck voltage (Figure 10a) and useful electrical power (Figure 10b) as a function of lines geometry.

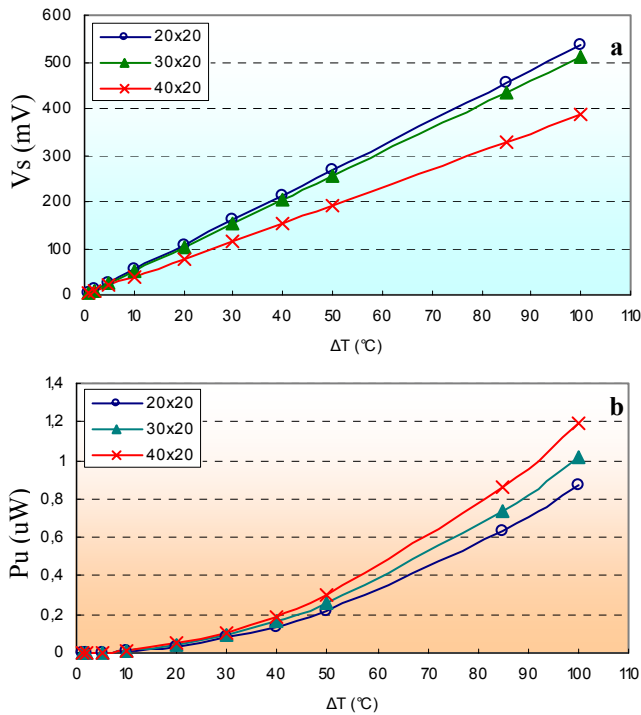


Figure 10: Seebeck voltage V_s evolution (a) and useful electrical power P_u evolution (b) as a function of temperature gradient and geometry.

For the Seebeck voltage, as explained before, we obtain the best value (535mV for $\Delta T=100K$) for the device which has the highest junctions numbers (i.e. 20x20). On the contrary and as shown in Table 1, concerning P_u , we obtain the highest value (1.2 μW for $\Delta T=100K$) for the device which has the lowest junctions numbers (i.e. 40x20). These power values are low enough, mainly due to global electrical resistances, and device geometry.

Conclusions

Design and technological process steps were reviewed and thermoelectric device performances have been discussed. Different annealing conditions demonstrated their strong influence on improving Bi-Sb electrical resistivity and consequently increasing thermoelectric generator performances. Seebeck voltage and electrical power have shown a high voltage and low power density for each device geometry. This means that these configurations are not suitable to supply high power but are interesting for temperature sensors thanks to a good sensitivity in voltage.

Nevertheless, the process steps optimization performed during this work will guide us in our current study of 3D device geometries better adapted for higher power.

The design optimization, process steps and electrical characterization discussed will be taken into account in our current work with new high performance, environmentally friendly thermoelectric materials such as doped silicon and silicon germanium alloys.

References

1. Arms, S. W. *et al*, "Power management for energy harvesting wireless sensors," *SPIE's Annual International Symposium on Smart Structures and Smart Materials*, San Diego, CA, (2005).
2. Schaevitz, S. B., "A MEMS thermoelectric generator," *M. Eng. In Electrical and computer Science*, Massachusetts Institute of technology, Cambridge, MA, (2000).
3. Böttner, H. *et al*, "New thermoelectric Components using Microsystem technologies," *Journal of micro-electromechanical system*, Vol. 13, No. 3 (2004), pp. 414-420.
4. Nolas, G. S. *et al*, Thermoelectrics – Basic Principles and New Materials Developments, Springer, (2001).
5. Beutler, D. E. *et al*, "Localization and electron-electron intercalations effects in thin Bi wires and films," *Physical Review B*, Vol. 38, No. 1 (1988), pp. 8-19.
6. Yang, F. Y. *et al*, "Large Magnetoresistance of Electrodeposited Single-Crystal Bismuth Thin Films," *Science*, Vol. 284 (1999), pp. 1335-1337.
7. D.M. Rowe, Thermoelectrics Handbook – Macro to Nano, CRC Press, (2006), pp. 30.1-30.14.